SF 298 MASTER COPY KEEP THIS COPY FOR REPRODUCTION PURPOSES

REPORT DOCUMENTATION PAGE

Form Approved
OMB NO. 0704-0188

1. AGENCY USE ONLY *(Leave blank)*	2. REPORT DATE	3. REPORT TYPE AND DATES COVERED
	16 May 1996	Final (April 95 - Oct. 1995)

4. TITLE AND SUBTITLE
Dynamic Inelasticity of Polymer-Matrix Composites

5. FUNDING NUMBERS
DAAH 04-95-1-0168

6. AUTHOR(S)
Horacio Dante Espinosa

7. PERFORMING ORGANIZATION NAMES(S) AND ADDRESS(ES)
Purdue University
1282 Grissom Hall
West Lafayette, IN 47907-1282

8. PERFORMING ORGANIZATION REPORT NUMBER

9. SPONSORING / MONITORING AGENCY NAME(S) AND ADDRESS(ES)
U.S. Army Research Office
P.O. Box 12211
Research Triangle Park, NC 27709-2211

10. SPONSORING / MONITORING AGENCY REPORT NUMBER
ARO 34475.2-EG-II

11. SUPPLEMENTARY NOTES
The views, opinions and/or findings contained in this report are those of the author(s) and should not be construed as an official Department of the Army position, policy or decision, unless so designated by other documentation.

12a. DISTRIBUTION / AVAILABILITY STATEMENT
Approved for public release; distribution unlimited.

12 b. DISTRIBUTION CODE

13. ABSTRACT *(Maximum 200 words)*

A novel experimental configuration that can record projectile velocity histories and target back surface out-of-plane motion in penetration experiments has been developed. The technique was used to investigate failure mechanisms during ballistic impact of an S-2 glass fiber woven composite with 60% fiber volume fraction. Microscopy studies performed on recovered samples clearly show interply delamination, fiber breakage, ply inelasticity, and fiber kinking as the major failure modes in these composites. Recorded penetrator velocity histories indicate these failure mechanisms are rate dependent. Pressure-shear recovery experiments were performed to investigate the out-of-plane dynamic shear resistance of the composite. Microstructural analyses revealed that at low impact velocities, 2 GPa compressive stresses, matrix cracking and matrix-fiber debonding are the primary damage mechanisms. At higher impact velocities, 4 GPa compressive stresses, fiber microcracking becomes pronounced.

14. SUBJECT TERMS
fiber composites, penetration experiments, pressure-shear recovery, microscopy

15. NUMBER IF PAGES
35

16. PRICE CODE

17. SECURITY CLASSIFICATION OR REPORT	18. SECURITY CLASSIFICATION OF THIS PAGE	19. SECURITY CLASSIFICATION OF ABSTRACT	20. LIMITATION OF ABSTRACT
UNCLASSIFIED	UNCLASSIFIED	UNCLASSIFIED	UL

DISCLAIMER NOTICE

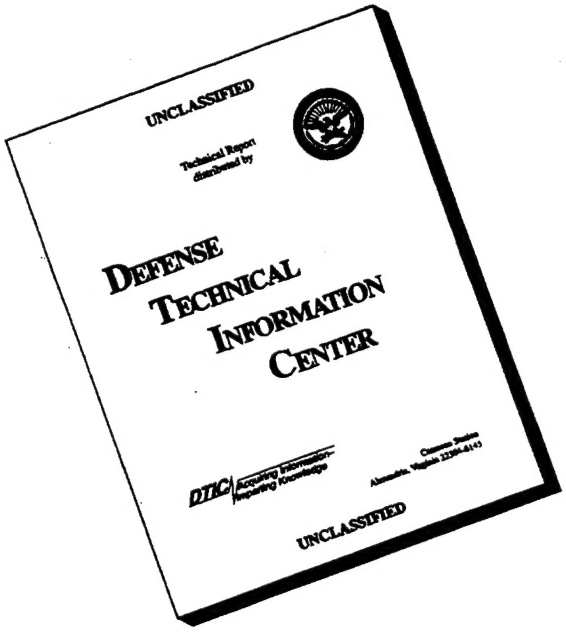

THIS DOCUMENT IS BEST QUALITY AVAILABLE. THE COPY FURNISHED TO DTIC CONTAINED A SIGNIFICANT NUMBER OF PAGES WHICH DO NOT REPRODUCE LEGIBLY.

DYNAMIC INELASTICITY OF POLYMER-MATRIX COMPOSITES

FINAL PROGRESS REPORT

HORACIO DANTE ESPINOSA

May 15, 1996

U.S. ARMY RESEARCH OFFICE

CONTRACT NUMBER: DAAH 04-95-1-0168

SCHOOL OF AERONAUTICS AND ASTRONAUTICS

West Lafayette, IN 47907-1282

TABLE OF CONTENTS

1. INTRODUCTION 3

2. PENETRATION EXPERIMENTS 6

2.1 Experimental Set-Up 6

2.2 Experimental Results: Velocity Measurements and Microscopy Study 7

3: PRESSURE-SHEAR RECOVERY EXPERIMENTS 21

3.1 Experimental Procedure 22

3.2 Experimental Results 23

4. FUTURE WORK 32

5. PARTICIPATING PERSONNEL 32

6. PUBLICATIONS 32

7. BIBLIOGRAPHY 32

1. INTRODUCTION

Fiber reinforced composite materials play an important role in civil and military applications through the design and manufacturing of advanced materials capable of attaining high stiffness/density and strength/density ratios. Presently, the utilization of glass fiber reinforced plastics (GRP) in the design of weight efficient armor systems and combat vehicle seems very promising. In these cases, analysis of structural integrity and dynamic response requires the understanding of material behavior under high loading rates. Of particular interest is the problem of damage initiation and evolution under a variety of loading states and deformation histories.

Impact damage in fiber-reinforced composite structures has received significant attention in the last decade since damage causes major strength losses. Insight into the failure mechanisms induced by impact damage in fiber-reinforced composite materials has been experimentally and computationally achieved, see Abrate 1991, 1994. The observed failure modes include delamination, interlaminar matrix cracking, fiber/matrix debonding, fiber breakage and fiber pull out, Cantwell, 1985; Elber, 1983. In general, low velocity impact results in matrix fracture and interply delamination. In high impact velocity experiments, another failure mode involving extensive fiber fracture is observed. Material failure depends on properties of the composite components which include the fibers, the matrix and the interface between plies. For instance, composites with higher fiber strength result in better impact resistance, Broutman, 1975.

Post-debond fiber sliding appears to be the primary energy absorbing mechanism in glass fiber-reinforced composites, Beaumont, 1979. The impact resistance of these composites did not depend on the matrix properties in high velocity impact tests conducted by Husman et al, 1975. Williams and Rhodes, 1982, found that the tensile performance of the matrix has a significant effect on impact behavior. Hunston, 1984, classified the link between matrix properties and fracture toughness. He showed that resin toughness is fully transferred to the toughness of the composite for brittle polymers, but for tougher polymers resin toughness is only partially transferred to the composite. The strength of the interface between matrix and fiber also plays an important role in the overall performance

of the composite. Dorey, 1980, showed that the transverse fracture energy of a composite depends significantly on the fiber/matrix bond strength.

Studies of impact damage, material dynamic properties and analysis of stress wave profiles generated by impact loading on an S-2 glass fiber-reinforced plastic composite are reported in Chou and DeLuca, 1993. The rate sensitivity of glass/epoxy laminates under tensile loading was investigated by Staab and Gilat, 1992. Their results indicate the maximum normal stress experienced by glass/epoxy laminates presents a mild rate sensitivity which is a function of the angle-ply fiber orientation. The compressive resistance of unidirectional GRP under high loading rate was examined by El-Habak, 1993. His experimental observations indicate that the failure mechanism is transverse tensile fracture due to fiber debonding and matrix tensile failure under both quasi-static and impact loading.

Lee and Sun, 1993a and b, studied the static and dynamic penetration of fiber composites. Experiments performed on AS4/polymer composites display damage initiating due the debonding followed by plug formation and pull-out of the plug. These penetration studies under quasi-static conditions were successfully incorporated into the analysis of projectile penetration.

Additional studies addressing the shear resistance of material when subjected to multiaxial dynamic loading are required for formulating a material model which can be used in numerical simulations. Studies addressing the effects of loading states, loading rates, and deformation histories are still limited. The material response at strain rates of the order of 10^5/sec is unexplored. Moreover, experiments in which the material is subjected to large inelastic deformations under high hydrostatic constraint have not been performed.

The present study concentrates on the comprehensive understanding of dynamic failure mechanisms in woven fiber-reinforced plastic laminates (GRP), made of S-2 glass fibers embedded in a polyester resin matrix with approximately 60% fiber by volume. The dynamic response of GRP composites subjected to ultra-high rates of deformation and multiaxial loading states from a micromechanical perspective is addressed. Pressure-shear recovery experiments were performed to examine the shear resistance of GRP and to understand the role of pressure on matrix inelasticity, and fiber-matrix interface behavior. Microscopy studies were performed on recovered samples to provide fundamental under-

standing of failure modes.

In addition to plate impact experiments, the penetration resistance of GRP was investigated in order to identify failure modes through direct measurement of impactor velocity and back surface velocity histories. Reverse penetration experiments were also performed to validate the penetrator velocity histories recorded in direct penetration experiments. Correlation between the damage mechanisms identified during plate impact experiments and in penetration experiments was achieved through microscopy studies performed on recovered composite samples.

2. PENETRATION EXPERIMENTS

In this chapter one of the main objectives of this investigation is presented. A new experimental configuration that can record projectile velocity histories and target back surface out-of-plane motion in penetration experiments has been developed. In many ballistic impact tests, often only the incident and residual velocities are recorded. To understand how targets defeat projectiles, the complete velocity history of the projectile must be recorded. Moreover, multiple instrumentation systems are highly desirable because they provide enough measurements for the identification of failure through modeling and analysis. We have developed an experimental technique using laser interferometry to measure the complete surface motion of both projectile and target plate.

2.1 Experimental Set-Up

Penetration experiments were conducted with a 3-in light gas gun with keyway at Purdue University. The experiments were designed to avoid complete destruction of the target plate such that microscopy studies could be performed in the samples. We have successfully measured impactor velocity and back surface velocity histories by using the set-ups shown in Figs. 1 and 2. The projectile holder was designed such that a normal velocity interferometer could be obtained on a laser beam reflected from the back surface of the projectile. In addition to this measurement, a multi-point velocity interferometer was utilized to continuously record the motion of the target back surface. It should be noted that the interferometric techniques used in this experiment have variable sensitivity so their resolution can be adjusted to capture initiation and evolution of failure. These records contain information on interply delamination history, fiber breakage and kinking, and matrix inelasticity.

In the case of direct penetration experiments, Fig. 1, a cylindrical target plate, 4-inch in diameter and 1-inch thick, was positioned in a target holder with alignment capabilities. The target was oriented so that impact at normal incidence was obtained. A steel penetrator, with a 30° conical tip, was mounted in a fiber glass tube by means of a PVC holder. This holder was designed so that two mirrors and a plano-convex lens could be placed along the path of a laser beam. In order to avoid projectile rotation that could

offset the interferometer alignment, a teflon key was placed in the middle of the fiber glass tube.

In the case of reverse penetration experiments, see Fig. 2, composite flyer plates were cut with a diameter of 2.25 inches and a thickness of 1 inch. In this case the flyer was mounted on a fiber glass tube by means of a backing aluminum plate. The penetrator, a steel rod with a 30° conical tip, was mounted on a target holder and aligned for impact at normal incidence. The penetrator back surface velocity was measured by means of NDI and NVI systems.

The projectile was accelerated down the keyway gun barrel by nitrogen gas filling a wrap around breech. An aluminum piston with two rubber O-rings was mounted to the rear end of the fiber glass tube to seal the wrap-around breech. The projectile velocity was measured by electronically recording the times of contact of four wire pins placed in the path of the projectile at the gun barrel exit. The first of the 1 Volt steps produced by the device was used to trigger a LeCroy 9784L oscilloscope. The photodetector outputs were then recorded on the oscilloscope as schematically shown in Figs. 1 and 2.

2.2 Experimental Results: Velocity Measurements and Microscopy Study

The impactor velocity during the penetration event, in experiment 5-1122, is given in Fig. 3. A velocity decrease of approximately 35 m/sec is observed after 100 μsec of the recorded impact. The velocity history of a point in the back surface at the specimen center, measured by means of a normal displacement interferometer (NDI), is shown in Fig. 4. A velocity increase to a value of 22 m/sec, followed by a decrease and increase to a maximum velocity of about 50 m/sec, after 20 μsec, is measured. In Fig. 5, the differential velocity between a point at the specimen center and another point, located 1 mm away from the specimen center, is shown. The objective of recording this relative normal velocity was to obtain information concerning the interply delamination velocity in the back of the target plate. This velocity was recorded by means of a differential displacement interferometer (DDI) and reveals a complex sequence of velocity changes. A maximum relative velocity of about 1.2 m/sec is recorded after 5.1 μsec of the wave arrival to the target back surface. Numerical simulations of the experiment are required to interpret the various features

observed in these velocity traces.

The recovered sample was examined under the microscope to identify the various failure modes experienced by the fiber composite during the penetration event. Three well defined regions with different failure zones are observed in the laminate, Fig. 6. In region A, at the rear of the target plate, extensive delamination between plies is seen leading to bulge formation. The delamination pattern exhibits some waveness, likely due to the morphology of the composite. A damage region is observed in front of the penetrator with substantial fiber shearing. The fibers appeared stretched in front of the projectile suggesting a membrane type of deformation that likely results in fiber tensile failure. Region B presents tensile fiber failure and large fiber deflection to accommodate the lateral expansion generated by the steel penetrator. Delamination is observed although in lesser degree than in Region A. Region C, at the projectile entrance, does not show extensive fiber deflection. Fiber microfracture followed by fiber tensile failure is believed to be the failure mode in this region. Noticeable delamination is also produced in plies close to the front specimen surface. It is seen that a variety of failure modes is produced during penetration of thick laminates. The precise sequence of events and stresses leading to these failures can only be identified through 3-D numerical simulations of the penetration process. All measured velocity histories are instrumental in providing insight into the damage and failure processes.

In addition to delamination, impact causes fiber failures, matrix cracking, and fiber-matrix debonding. Optical micrographs taken at the boundary between Regions A and B show all these failure mechanisms, see Figs. 7 and 8. Two major fiber failures are observed in the micrographs, fiber kinking and microcracking. In Fig. 7 a well defined kink band, on a ply with fibers oriented perpendicular to the penetration direction, is seen. The formation of kink bands appeared to be the result of compressive failure due to lateral motion of the plies away from the advancing steel penetrator. Many kink bands were observed in Regions B and C, but none was observed in Region A.

Fiber bending and large rotations are observed in Fig. 8. A typical failure mode with fiber shearing and deflection is seen in the lower ply. Interply delamination seems to assist these types of instabilities when the plies are moved laterally by the projectile. It should

be noted that in these figures the gap between 0°/90° is filled with glue. The glue was added during the sample preparation to avoid further damage in the composite sample. Two SEM pictures showing details of the fiber failure are shown in Figs. 9 and 10. The extent of the bending and the periodic formation of L and T-shaped cracks can be observed in Fig. 10. The microcrack spacing is approximately 30-40 μm. These microcracks appear to initiate in the tensile region of the fiber propagating in a direction perpendicular to the fiber axis. A change in crack propagating direction is observed when the crack approaches the compressive region within each fiber. At this stage, crack extension parallel to the fiber axis is seen. This failure mechanism is consistent with the independent bending of each fiber, likely resulting from debonded fiber-matrix interfaces.

Shown in Figs. 11 and 12 are SEM micrographs of a kink band. A band width of approximately 250 μm is observed. The matrix has a granular appearance and presents large amounts of inelasticity. Extensive fiber-matrix debonding is seen with matrix material attached to the fiber surface. These features together with the granular appearance of the polymer matrix suggest heating and quenching of the polymer.

In order to examine the extent of damage in 90° plies, SEM micrographs were taken in Region B, 100 μm, 300 μm, and 1000 μm away from the penetrator cavity, see Figs. 13, 14, and 15, respectively. Extensive fiber cracking and matrix-fiber debonding is observed in the region close to the penetrator cavity. Matrix cracking with large openings and moderate fiber cracking is observed 300 μm away from the penetrator. This feature is consistent with the observations previously shown in Figs. 7 and 8. In a region 1000μm away from the penetrator cavity, no fiber fracture and a mild fiber-matrix debonding is observed. These features show ply damage is mainly contained in a region with a width of approximately half the penetrator diameter on each side of the penetrator cavity. By contrast, interply delamination is extended several diameters away from the penetrator and in Region A involves the entire 4-inch target diameter.

In order to confirm the velocities measured in the direct penetration experiment, we conducted two reverse penetration experiments at impact velocities of 200 and 500 m/sec, experiments 6-0308 and 6-0314, respectively. Another objective of these experiments was to examine rate effects in the penetration resistance of woven fiber composites. The inter-

ferometrically measured penetrator velocities are plotted in Fig. 16. The steel penetrator velocity shows a progressive increase and a decrease to almost zero velocity upon arrival of an unloading wave generated at the penetrator free surface. The arrival time of approximately 14 μsec coincides with the round trip time of the wave through the penetrator tip back to the penetrator free surface. This feature is observed in both experiments. A continuous increase in velocity is recorded with velocities of 20 m/sec and 32 m/sec after 42 μsec, respectively. A maximum velocity of 50 m/sec is recorded in experiment 6-0314 after 65 μsec. A comparison of the velocity histories in these two experiments clearly reveals the composite failure presents a moderate rate sensitivity. Moreover, the velocities recorded in experiment 6-0308 appear to confirm the velocity reduction interferometrically recorded in experiment 5-1122 (direct penetration experiment).

It should be noticed that in the case of direct penetration the composite sample had a diameter of 4 inches, while, in the case of the reverse penetration experiment the composite sample had a diameter of 2.25 inches. Based on the microscopy study previously reported, it is clear that the major difference between the 4 and 2.25-inch samples, is in the extent of interply delamination. As noted earlier, damage and failure during the penetration event is confined to a dimension of approximately one projectile diameter. Likely, this is the reason for the reasonable agreement between direct and reverse projectile velocity measurements. More experiments are needed to confirm these findings.

Figure Captions

Figure 1: Experimental set-up for *direct* penetration experiments.

Figure 2: Experimental set-up for *reverse* penetration experiments.

Figure 3: Penetrator axial velocity recorded in experiment 5-1122.

Figure 4: Normal velocity history of a point in the back surface at the center of the composite target, experiment 5-1122.

Figure 5: Relative axial velocity between two points separated by 1 mm at the back surface of the composite target, experiment 5-1122.

Figure 6: Optical micrograph of recovered composite sample from direct penetration experiment 5-1122. Three regions with different failure modes are observed. The half inch diameter penetrator provides a scale for this micrograph.

Figure 7: Optical micrograph taken at the boundary between Regions A and B. Fiber kinking and matrix cracking are observed in 0° and 90° plies, respectively.

Figure 8: Optical micrograph taken at the boundary between Regions A and B. Fiber shearing and bending with large displacements and rotations are observed.

Figure 9: SEM micrograph showing details of fiber bending and cracking.

Figure 10: High magnification SEM micrograph, from the region shown in Fig. 9, indicating the formation of periodic L and T-shaped microcracks within the S-2 glass fibers.

Figure 11: SEM micrograph of a typical kink band showing a band width of approximately 250 μm.

Figure 12: High magnification SEM micrograph, from the region shown in Fig. 9, displaying extensive fiber-matrix debonding and granular appearance of the polymer matrix.

Figure 13: SEM micrograph of a 90° ply taken in Region B, at 100 μm from the penetrator cavity. Severe fiber cracking and matrix-fiber debonding is observed.

Figure 14: SEM micrograph of a 90° plie taken in Region B, at 300 μm from the penetrator cavity. Matrix cracking with large openings is observed.

Figure 15: SEM micrograph of a 90° plie taken in Region B, at 1000 μm from the penetrator cavity. No fiber breakage and small fraction of debonded fiber-matrix interphases is observed.

Figure 16: Penetrator velocity histories from experiments 6-0308 and 6-0314.

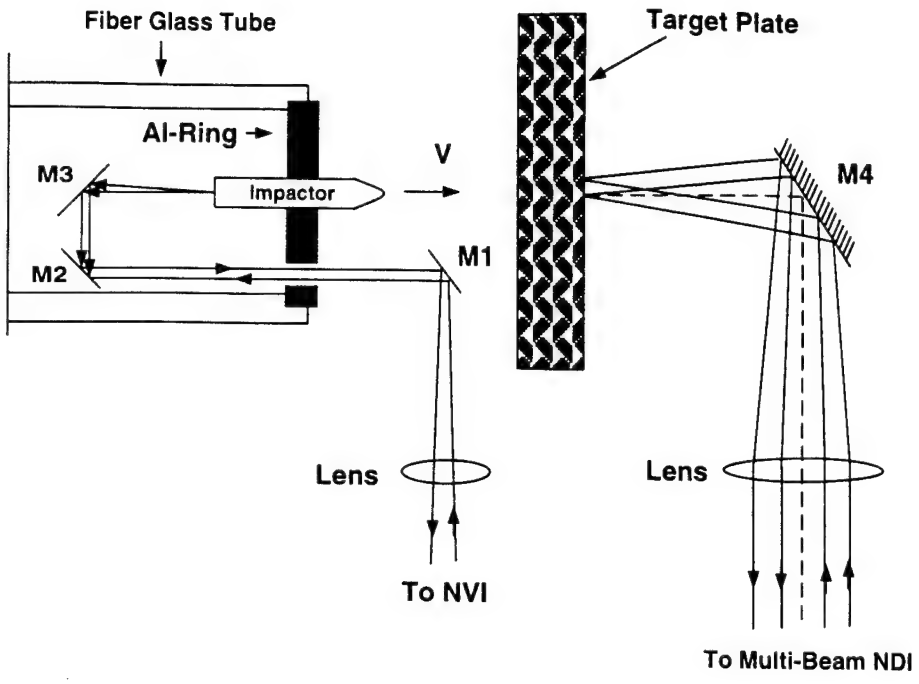

Figure 1.

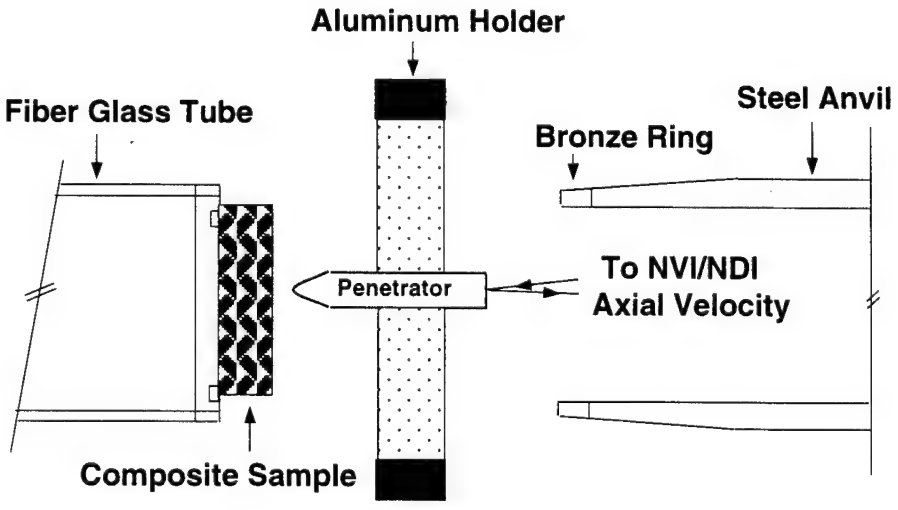

Figure 2.

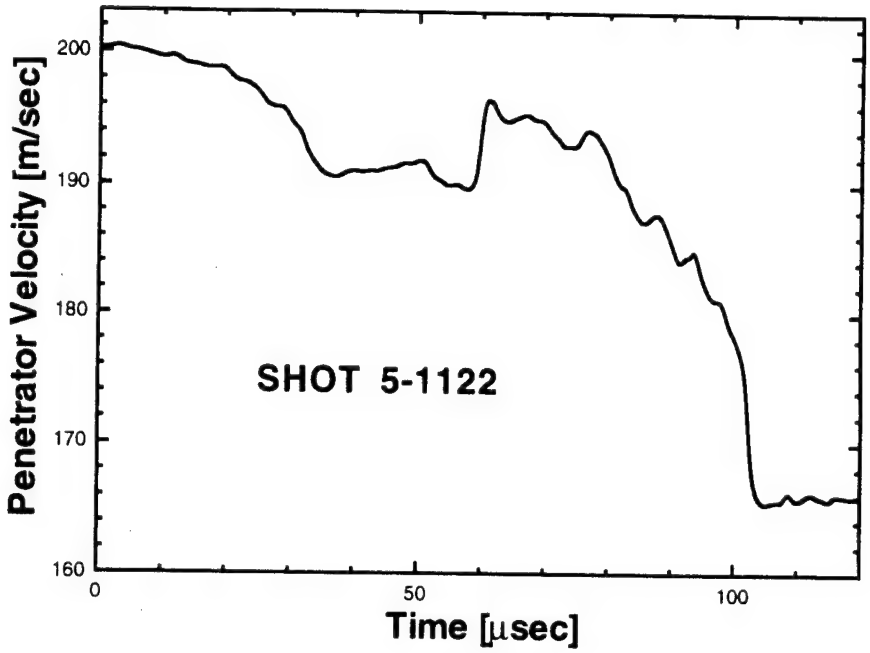

Figure 3.

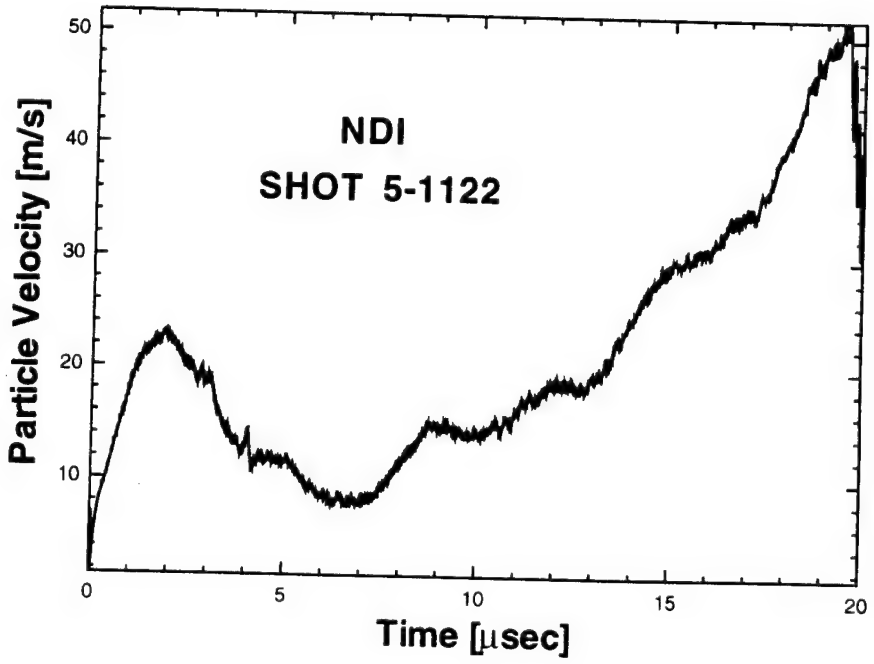

Figure 4.

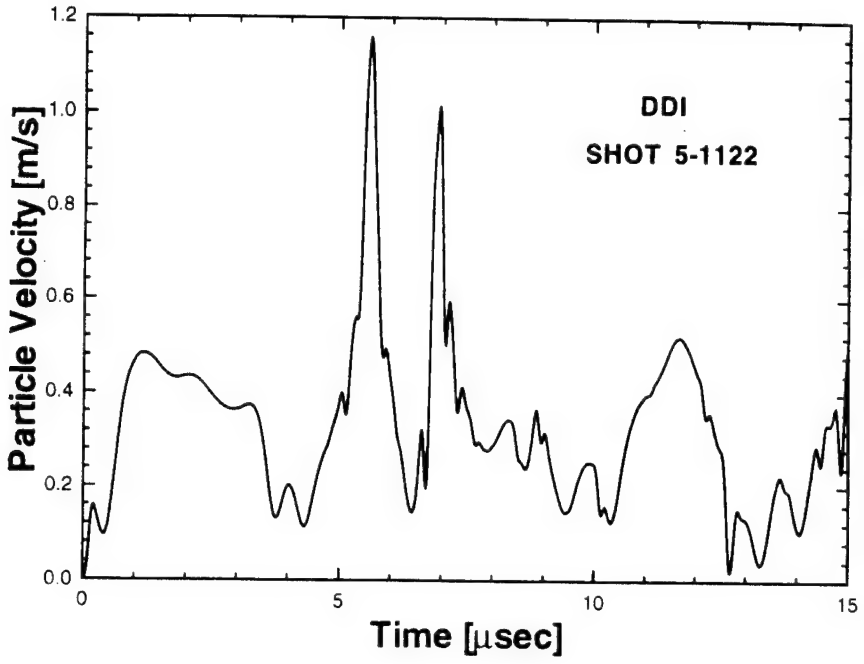

Figure 5.

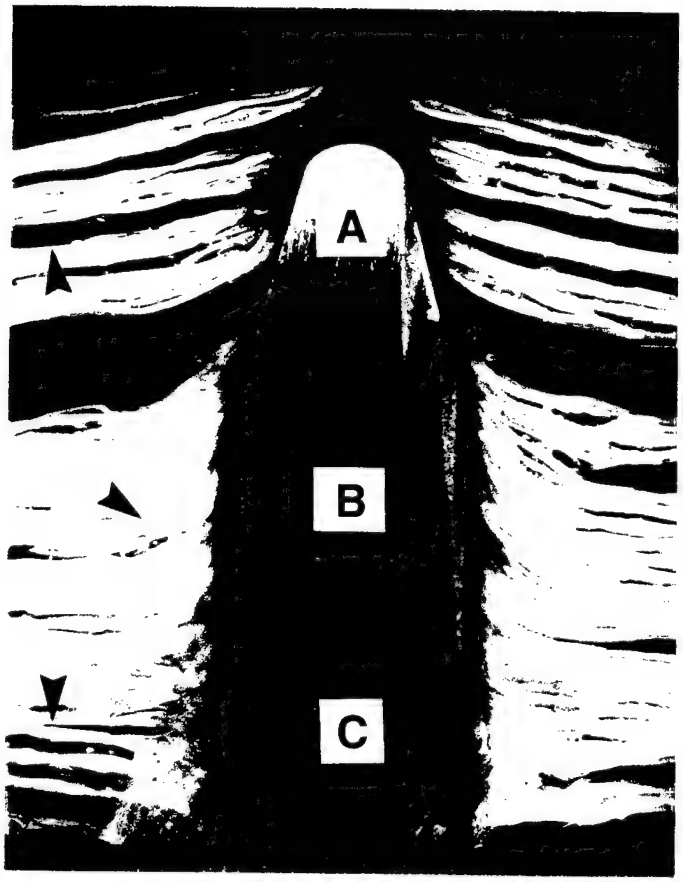

Figure 6.

Figure 7.

Figure 8.

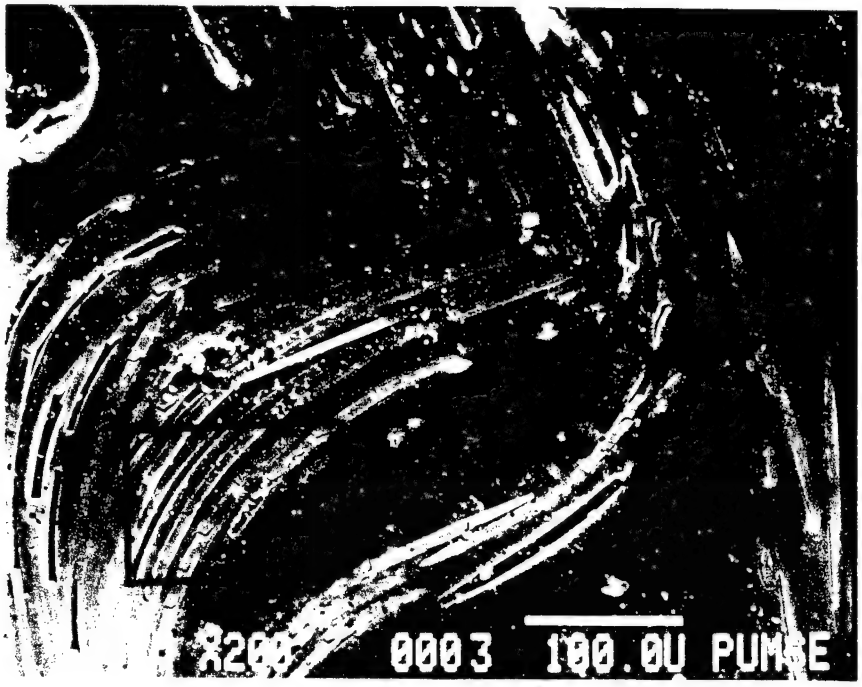

Figure 9.

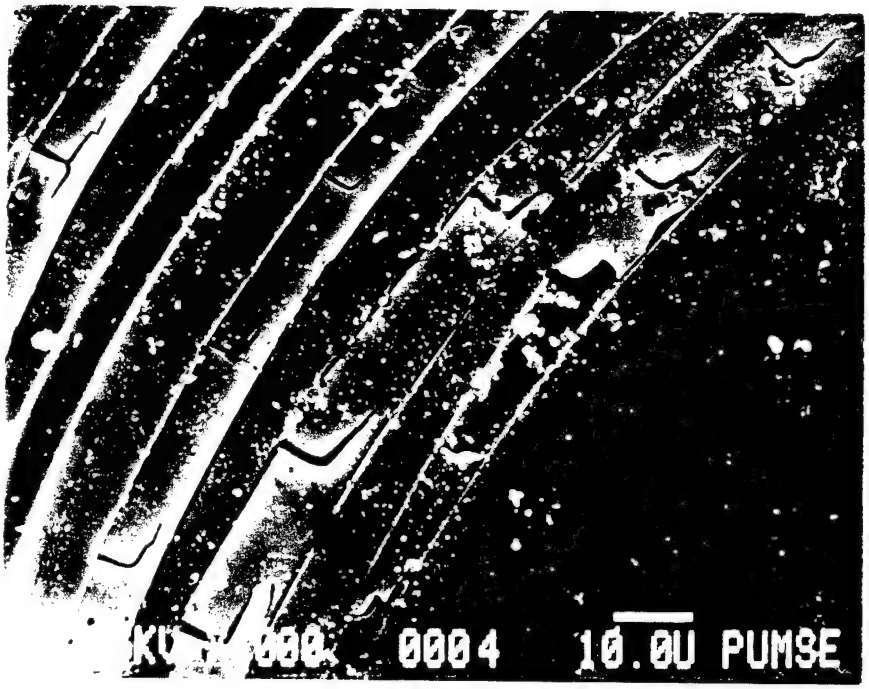

Figure 10.

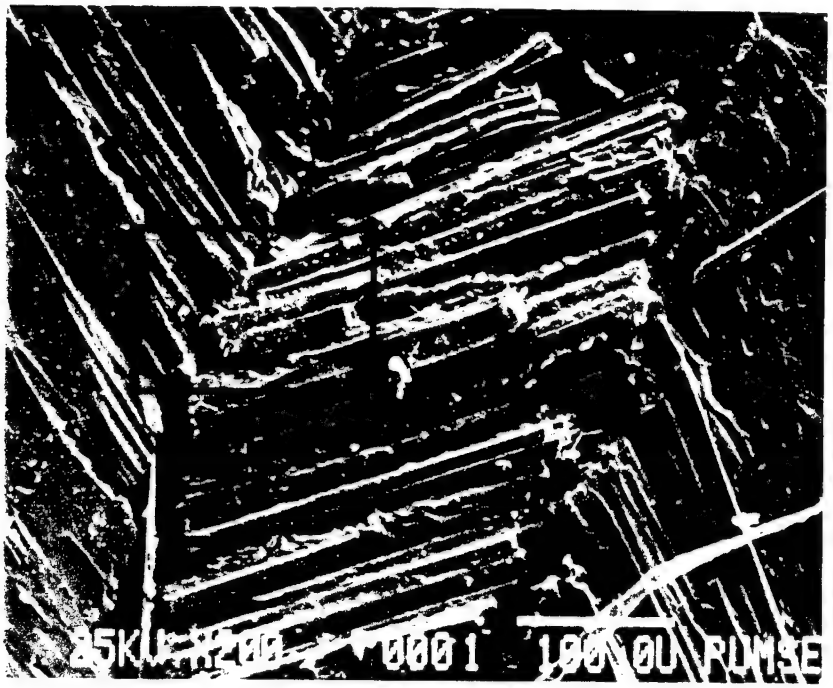

Figure 11.

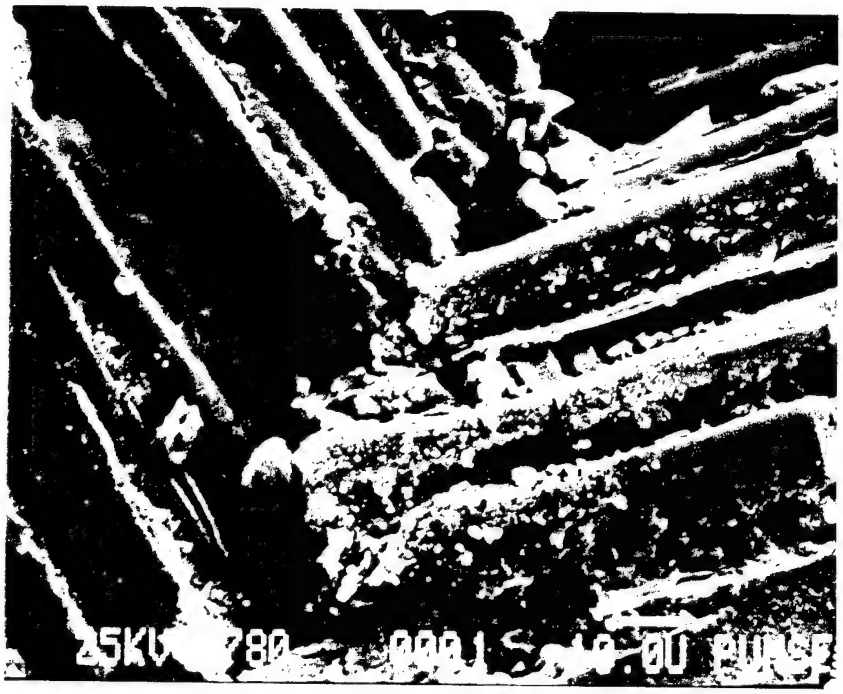

Figure 12.

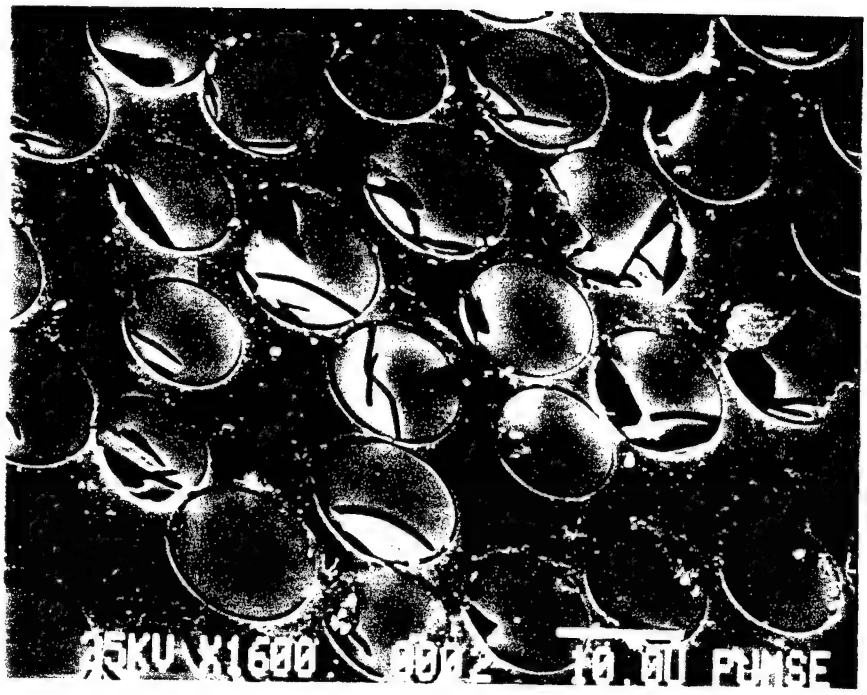

Figure 13.

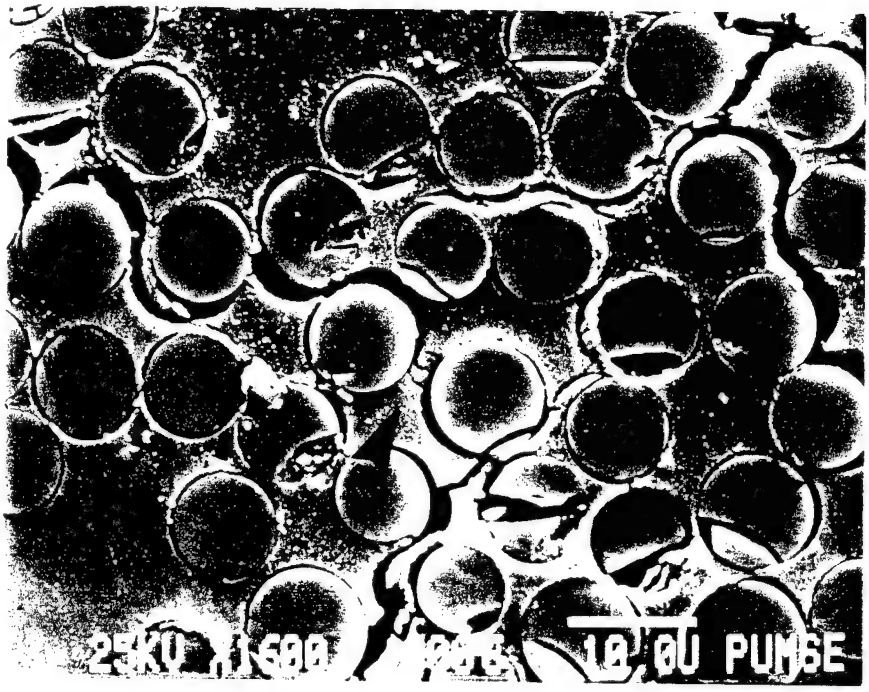

Figure 14.

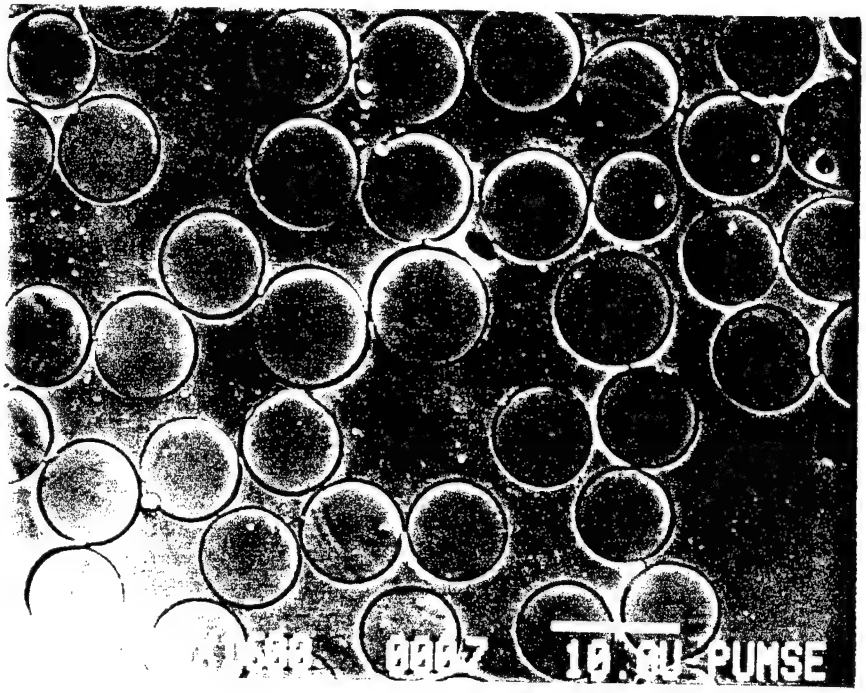

Figure 15.

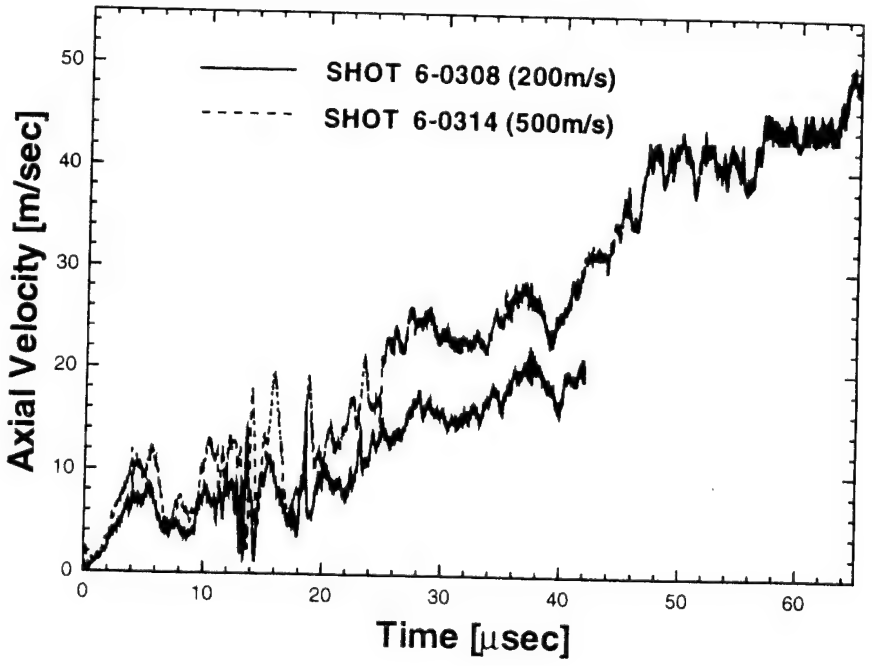

Figure 16.

3. PRESSURE-SHEAR RECOVERY EXPERIMENTS

As previously discussed, severe out-of-plane shearing occurs within laminates in penetration experiments. Particularly, extensive matrix microcracking and fiber-matrix debonding is observed between kink bands. In order to investigate the high strain rate shear resistance of the material, pressure shear recovery experiments were conducted.

Plate impact experiments offer unique capabilities for the characterization of advanced materials under dynamic loading conditions (Espinosa and Clifton, 1991). These experiments allow high stresses, high pressures, high strain rates and finite deformations to be generated under well characterized conditions. The testing techniques can be divided into two categories: a) stress wave propagation tests (pressure-shear symmetric impact and soft-recovery normal impact) and b) nominally homogeneous deformation tests (pressure-shear sandwich configuration). They all rely on the generation of one-dimensional waves in the central region of the specimen in order to allow a clear interpretation of the experimental results and the mathematical modeling of the material behavior. Pressure shear recovery experiments, Espinosa et al., 1995, offer several advantages over other experimental techniques in the study of damage and inelasticity in metals, ceramics, and composite materials. The stress amplitudes and deformation rates obtained in these experiments allow the identification of microcracking and shear localization. Furthermore, the information gathered from these experiments is substantially increased by correlation of real-time velocity profiles and microstructural features associated with the mechanisms of inelasticity and damage.

Compression-shear loading is attained by inclining the flyer and target plates with respect to the axis of the projectile. By varying the angle of inclination a variety of loading states may be achieved. The configuration is shown in Fig. 17.

One of the problems associated with the pressure-shear recovery experiment is the simultaneous trapping of the longitudinal and shear momentum by a back plate. To solve this problem, this investigation uses a multi-plate flyer (Espinosa, 1992). Such a flyer consists of a thin film made of a material with a very low shear flow stress (e.g., a polymer), sandwiched between two thicker hard plates. Due to the mismatch in impedances between

the thin film and the anvil plates, a few reverberations are required to achieve the shear stress imposed at the impact face. This requires a very thin film to minimize the time required to achieve a homogeneous state. We have manufactured such a multi-plate flyer by bonding two hard plates with a uniform 1 μm-thick polymer layer.

3.1 Experimental Procedure

The pressure-shear recovery experiments were carried out in a 3.0-inch gas gun at Purdue University. The multi-plate impactor and target plates were made of speed-star steel, while the glass fiber-reinforced plastic laminates were made of S-2 glass fibers embedded in a polyester resin matrix with approximately 60% fiber by volume. The dimensions of the plates were chosen such that the first unloading wave from the periphery arrived at the point of measurement later than the unloading shear wave. The steel plates and composite wafer were lapped flat using 15 μm silicon carbide powder slurry. This was done to a flatness better than 3 rings, measured by means of a Newton interferometer. Before mounting the composite specimen, the surface of the multi-plate flyer was roughened to provide sufficient surface roughness to transfer the in-plane motion without sliding.

The composite specimen was clamped to a multi-plate flyer, then a small amount of epoxy was applied around the periphery to fix the composite in place. The two pieces were clamped tightly to avoid penetration of the epoxy into the specimen-flyer interface. A thin layer of aluminum was then vapor-deposited on part of the impact face of the specimen to provide an electrically conductive surface for later measurement of any misalignment between target and impactor.

The impactor was glued to the front end of a fiberglass tube with the impact plane skewed from the axis of the tube at an angle of 18 degrees. An aluminum piston with two rubber O-rings was mounted to the rear end of the tube to seal the wrap-around breech. A key was also mounted on the middle of the fiber glass tube to prevent rotation of the projectile.

After the target plate was mounted in the holder ring, it was aligned to the face of the projectile within 0.5 milliradians using the optical technique developed by Kumar and Clifton (1977). In order to check the angle of misalignment at impact, four copper

pins were mounted on the target plate. At impact, these pins contacted the deposited aluminum film on the composite specimen, resulting in four voltage steps, in the ratio of 1:2:4:8, which were recorded in a Tektronix DSA 602A oscilloscope. The projectile velocity was measured by recording the times of contact of four wire pins placed in the path of the projectile.

The target rear surface was polished and then a thin layer of positive photoresist was deposited using a spinning machine. A holographic phase grating was constructed by interference of two laser beams. The angle between the beams was selected such that a sinusoidal profile with 1000 lines/mm was obtained. This grating was utilized to measure the normal and transverse displacements by means of a Variable Sensitivity Displacement Interferometer (VSDI) (Espinosa et al.,1995). A schematic of the optical measuring system is shown in Fig. 18. The normally reflected beam is split at beamsplitter BS1; each half of the normal beam was then made to interfere with one of the diffracted beams via beamsplitters BS2 and BS3. The resulting signal generated by each interfering beam pair was monitored by photodetectors. The interferometric signals were recorded with avalanche silicon detectors manufactured by EG&G, with a bandwidth of 800 MHz, in a Tektronix DSA 602A oscilloscope with 1 GHz bandwidth.

Recovered samples were examined under a scanning electron microscope. The purpose of this SEM examination was to observe the damage induced in the composite by the high strain rate loading. Two different views of the sample were analyzed. The first was a micrograph of a delaminated surface parallel to the impact surface, while the other was a section view across the composite specimen. The section specimens were wet ground with 320, 400 and 600 grit silicon carbide paper, then polished with 10 μm, 3 μm, 0.1 μm alumina oxide slurries. Once they were well polished, the specimens were etched by 2.5 N HF for 15 seconds.

3.2 Experimental Results

Three shots have been completed using the experimental set up previously discussed. A summary of these shots is presented in TABLE 1. The normal velocity-time profiles obtained from these experiments are shown in Fig. 19. The normal particle velocity shows

a velocity reduction after the initial jump indicating the presence of a small gap between the GRP composite and the multi-plate flyer. Comparing these shots, we can observe that the gap in shot 5-0512 is smaller than that of shots 5-0621 and 5-0717. However, since the most important part of the trace is in the state of homogeneous deformation that develops after the transient state, the existence of a small gap at the specimen-impactor interface does not appear to affect the interpretation of the experimental records. In shot 5-0512 the velocity rises upon the reverberation of waves within the specimen to a velocity of about 90 m/sec, at approximately 1.1 μsec. It is followed by a reduction and increase in velocity due to wave reverberations in the thin layer used in the multi-plate flyer. An approximately constant velocity of 100 m/sec is monitored in the next 1.1 μsec, followed by an unloading wave at approximately 2.2 μsec. The peak normal stress in this shot reaches 2.7 GPa. For shots 5-0621 and 5-0717, the normal velocity follows similar histories with a maximum velocity of 170 m/s corresponding to a stress level of approximately 4.2 GPa.

The transverse particle velocity history shown in Fig. 20 shares some of the characteristics of the normal velocity. For shot 5-0512 the transverse particle velocity reaches 15 m/sec after 600 nsec of the wave arrival to the target back surface. The shear stress progressively increases to its maximum value of 200 MPa. After 1.5 μsec the velocity trace shows a progressive reduction indicating material damage. For the higher velocity shots, 5-0621 and 5-0717, the softening rate is much higher after peak shear stresses of 240 MPa and 270 MPa are attained, respectively. This appears to indicate that in both shots, the pressure-shear loading is producing significant inelastic deformation in the material. The damage mechanisms responsible are examined through SEM micrographs.

Microscopy studies on an untested specimen were conducted to assure that damage was not present before the experiment. No microcracking was found. Occasionally, some debonding was found between the fiber and the matrix. This debonding was probably due to the thermal mismatch between constituents. It is known that thermal stresses developed, in the vicinity of the fiber/matrix interface, upon cooling from the curing temperature down to room temperature during manufacturing.

A section micrograph of the recovered composite sample, shot 5-0512, is shown in Fig. 21. Transverse shear cracks are observed crossing the thickness of the sample. Such

cracks are consistent with the multiaxial state of stress induced by shear impact loading. A closer look at the composite microstructure, see Fig. 22, portrays a high frequency of debonding at the fiber-matrix interfaces. Also, formation of well-defined inelastically deformed regions within the matrix, possibly along surfaces of maximum shear stress, are observed.

With the increase in impact velocity, fiber cracking initiates, see Figs. 23 and 24. The higher axial stress generated in these experiments, shots 5-0621 and 5-0717, leads to fragmentation in the S-2 glass fibers. Although the bulk stresses would not be high enough to damage the fibers, the local stress concentrations appear to be severe enough to cause not only matrix cracks and interfacial debonding, but also failure within the fibers.

Shot No.	Specimen/ Thickness $[mm]$	Impactor/ Thickness $[mm]$	Target/ Thickness $[mm]$	Projectile/ Velocity $[m/sec]$	Tilt [mrad]	Normal Stress [GPa]
95-0521	0.31	2.40/3.3	6.45	132	1.5	2.7
95-0621	0.32	2.59/3.20	7.05	194	2.0	4.2
95-0717	0.25	3.16/3.58	6.9	189	1.95	4.1

TABLE 1. Summary of Experiments

Figure Captions

Figure 17: a) Pressure-shear recovery configuration, b) Lagrangian X-t diagram of pressure-shear experiment according to 1-D elastic wave theory.

Figure 18: Optical layout of VSDI system. The $\Theta^{\pm}$ VSDI system is obtained by combining a normally reflected beam and a diffracted beam at an angle $\theta^{\pm}$.

Figure 19: Normal velocity histories from pressure-shear experiments 5-0512, 5-0621, and 5-0717.

Figure 20: Transverse velocity histories from pressure-shear experiments 5-0512, 5-0621, and 5-0717.

Figure 21: Optical micrograph of recovered composite sample from experiment 5-0512.

Figure 22: SEM micrograph of recovered composite sample, Shot 5-0512, showing fiber-matrix debonding, matrix inelasticity.

Figure 23: SEM micrograph of recovered composite sample, Shot 5-0621, showing fiber-matrix debonding, matrix inelasticity, and fiber microcracking.

Figure 24: SEM micrograph of recovered composite sample, Shot 5-0717, showing fiber-matrix debonding, matrix inelasticity, and fiber microcracking.

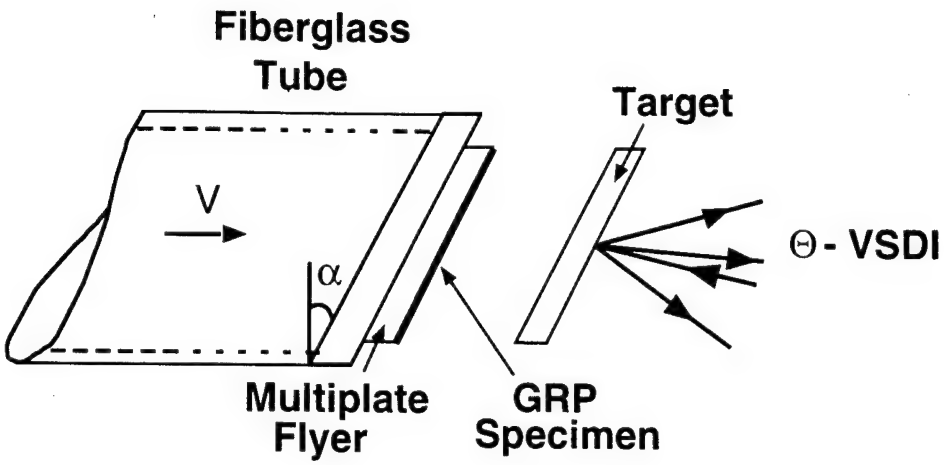
Fiberglass
Tube
Target
V
α
Θ - VSDI
Multiplate
Flyer
GRP
Specimen

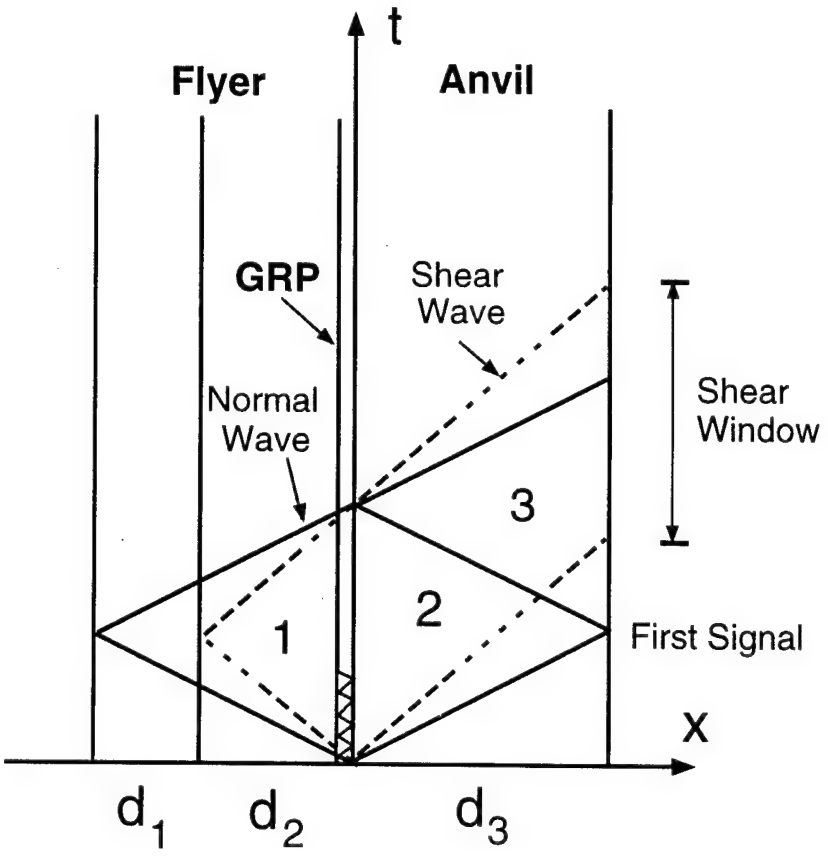
t
Flyer
Anvil
GRP
Shear
Wave
Normal
Wave
Shear
Window
3
2
1
First Signal
x
d1
d2
d3

Figure 17.

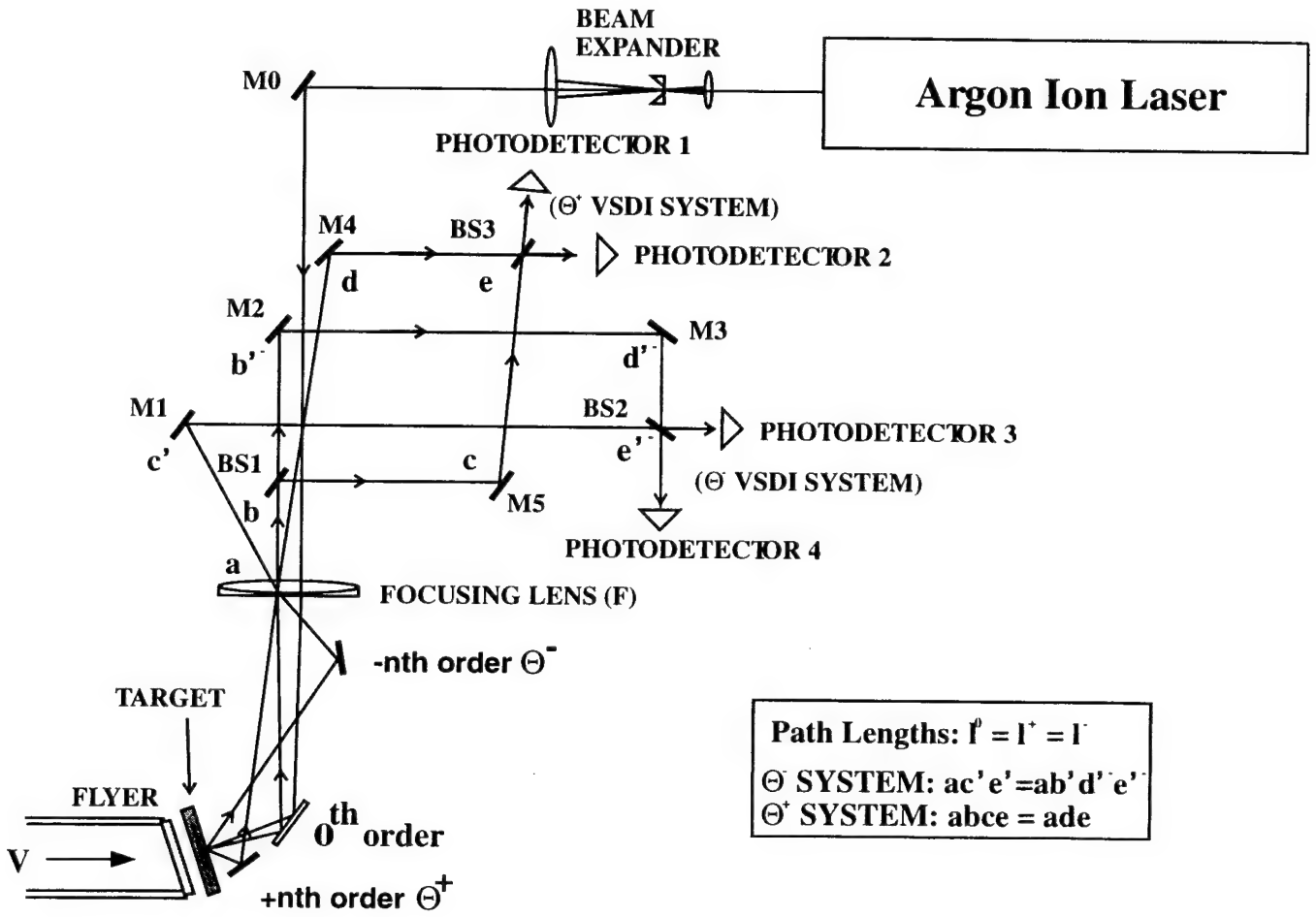
BEAM
EXPANDER
M0
Argon Ion Laser
PHOTODETECTOR 1
(Θ+ VSDI SYSTEM)
M4
BS3
PHOTODETECTOR 2
d
e
M2
M3
b'
d'
M1
BS2
PHOTODETECTOR 3
c'
BS1
c
e'
(Θ- VSDI SYSTEM)
b
M5
PHOTODETECTOR 4
a
FOCUSING LENS (F)
-nth order Θ-
TARGET
Path Lengths: l' = l+ = l-
Θ- SYSTEM: ac'e'=ab'd'e'
Θ+ SYSTEM: abce = ade
FLYER
0th order
V
+nth order Θ+

Figure 18.

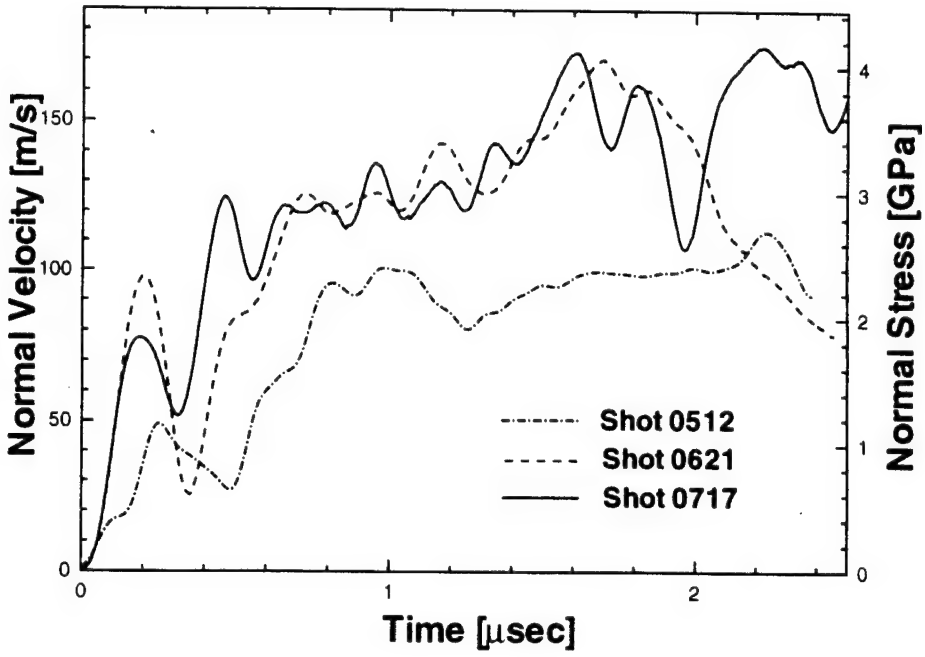

Figure 19.

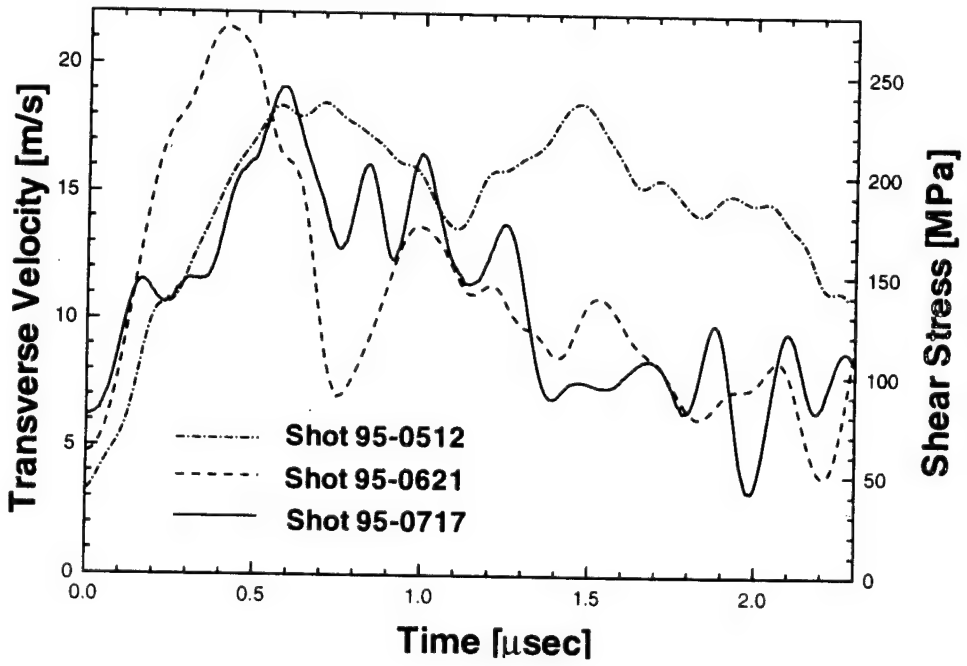

Figure 20.

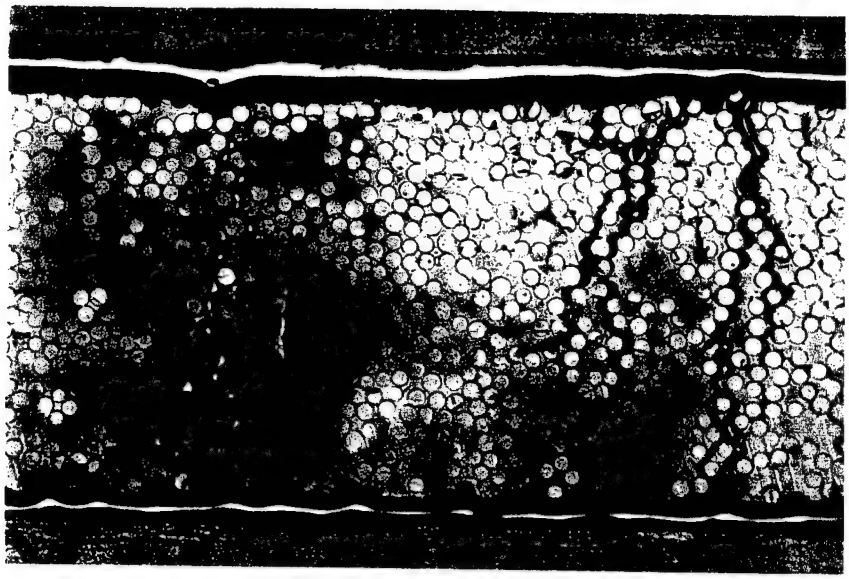

Figure 21.

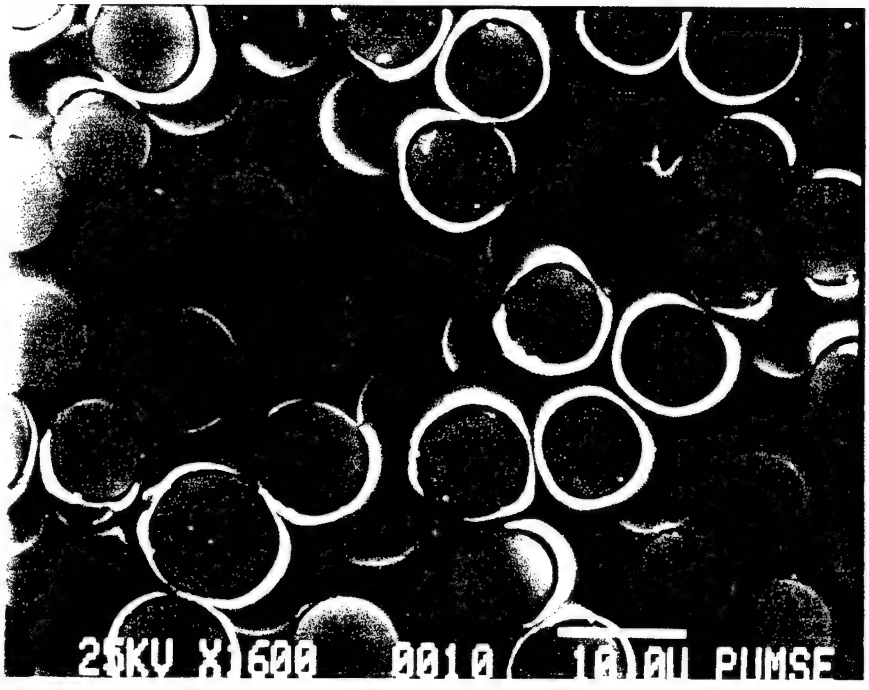

Figure 22.

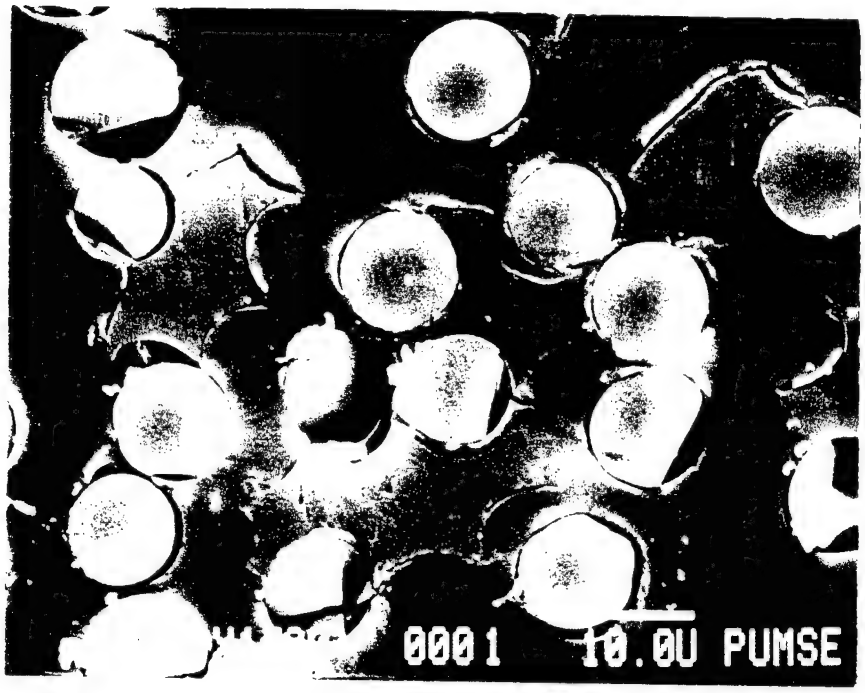

Figure 23.

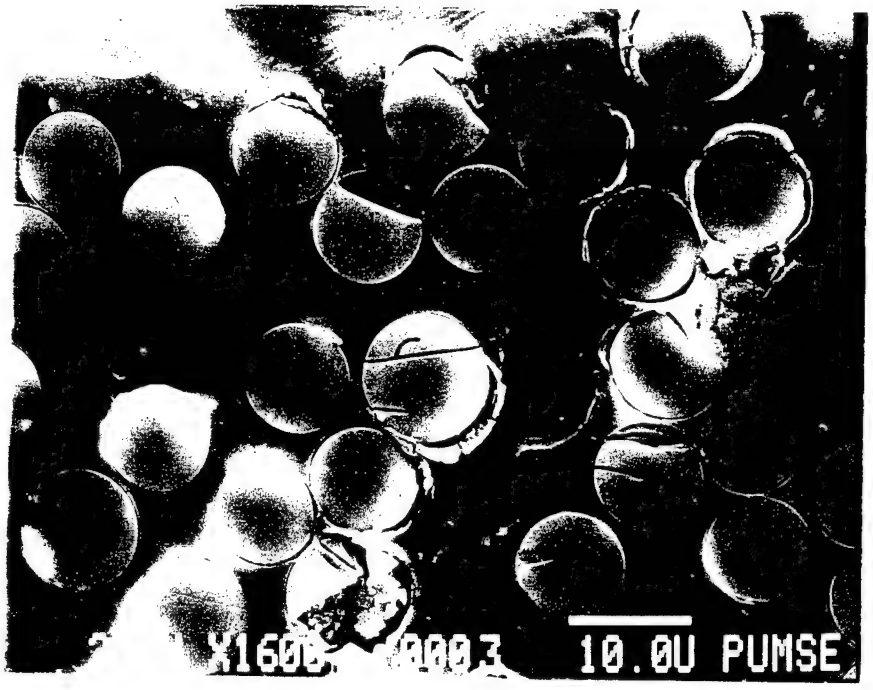

Figure 24.

4. FUTURE WORK

Future work will focus on the comprehensive understanding of failure mechanisms and the formulation of physically based models. A numerical algorithm to simulate penetration experiments in composite targets will be developed. A Lagrangian FEM with dynamic contact, and finite deformation capabilities is currently under development. The contact law has been augmented with a decohesion law to simulate delamination and friction between plies.

5. PARTICIPATING PERSONNEL

Two graduate students, Hung-Chen Lu and Yueping Xu, participated in this project. Mr. Lu is a Ph.D. student that has successfuly completed all the course work and exams. He expects to graduate in May of 1997. Mrs. Xu is a Master student expecting to graduate in May of 1997.

6. PUBLICATIONS

- Espinosa, H.D., Emore, G., and Xu, Y., 1995, "High Strain Rate Behavior of Composites with Continuous Fibers", ASME Special Technical Publication, *High Strain Rate Effects on Polymer, Metal and Ceramic Matrix Composites and Other Advanced Materials*, edited by Y.D.S. Rajapakse and J.R. Vinson, San Francisco, California, pp. 6-16.

7. BIBLIOGRAPHY

- Abrate, S., 1991,"Impact on Laminated Composite Materials," *Applied Mechanics Review*, Vol. 44(4), pp. 155-190
- Abrate, S., 1994,"Impact on Laminated Composites: Recent Advances," *Applied Mechanics Review*, Vol. 47(11), pp. 517-544
- Arcan, M., Hashin, Z., and Voloshin, A., 1978, "A Method to Produce Uniform Plane Stress States with Applications to Fiber Reinforced Materials," *Exp. Mech.*, Vol. 18, pp. 141-146.

- Beaumont, P.W.R., 1979,"Fracture Mechanisms in Fibrous Composites," in Fracture Mechanics, Current Status, Fracture Prospects edited by R. A. Smith (Pergamon Press), pp. 211-233.
- Broutman, LJ., and Rotem, A., 1975,"Impact Strength and Toughness of Fiber Composite Materials," in Foreign Object Impact Damage to Composites, ASTM STP568 *American Society for Testing and Materials*, pp. 114-133.
- Cantwell, W.J., 1985,"Impact Damage in Carbon Fiber Composites," Ph.D Thesis, University of London, U.K.
- Chou, S-C, and Deluca, E., 1993,"Dynamic Response of S- 2 Glass Reinforced Plastic Structural Armor," Report No. ARL-SR-5.
- Cuitiño, A. and Ortiz, M.,1992,"A Material-Independent Method for Extending Stress Update Algorithms From Small-Strain Plasticity to Finite Plasticity With Multiplicative Kinematics," *Engineering Computations*, Vol. 9, 437-451.
- Dorey, G., 1980,"Relationship between Impact Resistant and Fracture Toughness in Advanced Composite Materials," in Effect of Service Environment on Composite Materials, *AGARD CP 28*
- Elber, W., 1983,"Failure mechanics in Low Velocity Impact on Thin Composite Plates," *NASA Techical Paper 2152.*
- El-Habak, A.M., 1993,"Compressive Resistance of Unidirectional GFRP Under High Rate of Loading,"*J. of Composites Technology and Research*, Vol. 15, pp. 311-317.
- Espinosa, H.D., 1992, "Micromechanics of the Dynamic Response of Ceramics and Ceramic Composites", Ph.D. Thesis, Brown University, Providence, RI.
- Espinosa, H.D. and Clifton, R.J., 1991,"Plate Impact Experiments For Investigating Inelastic Deformation and Damage of Advanced Materials," In: K-S. Kim editor, *Experiments in Micromechanics of Failure Resistant Materials*, AMD-130, pp. 37-56, ASME.
- Espinosa, H.D., Mello, M. and Xu, Y., 1995,"A Variable Sensitivity Displacement Interferometer with Application to Wave Propagation Experiments," Submitted to *J. Appl. Mech.*
- Espinosa, H.D., Emore, G., and Xu, Y., 1995, "High Strain Rate Behavior of Com-

posites with Continuous Fibers", ASME Special Technical Publication, *High Strain Rate Effects on Polymer, Metal and Ceramic Matrix Composites and Other Advanced Materials*, edited by Y.D.S. Rajapakse and J.R. Vinson, San Francisco, California, pp. 6-16.

- Ha, S.K., Wang, Q. and Chang, F-K., 1991,"Modeling the Viscoplastic Behavior of Fiber-Reinforced Thermoplastic Matrix Composites at Elevated Temperatures," *Journal of Composite Materials*, Vol. 25, pp. 334-374.
- Hunston, D.L., 1984,"Composite Interlaminar fracture ; Effect of matrix Fracture Energy," *Composites Tech Review 6*, pp. 176-180.
- Husman, G.E. and Whitney, J.M.and Halpin, J.C., 1975,"Residual strength Characterization of Laminated Composites Subjected to Impact Loading," in foreign Object Impact Damage to Composites, *American Society for Testing and materials. STP 568*, pp. 92-113.
- Kumar, P. and Clifton,R.J., 1977,"Optical Alignment of Impact Faces for Plate Impact Experiments,",*J. Appl. Physics*, Vol. 48, pp. 1366-1367.
- Lee, S-W. R., and Sun, C.T., 1993a,"A Quasi-Static Penetration Model for Composite Laminates,"*J. of Composite Materials*, Vol. 27, pp. 251-271.
- Lee, S-W. R., and Sun, C.T., 1993b,"Dynamic Penetration of Graphite/Epoxy Laminates Impacted by a Blunt-Ended Projectile," *Composites Science and Technology*, Vol. 49, pp. 369-380.
- Seaman, L., 1989, "Rotation Transformations for Two-Dimensional Calculations," *Int. J. Solids and Structures*, Vol. 7, pp. 735-750.
- Staab, G.H. and Gilat, A., 1992,"Behavior of Angle-Ply Glass/Epoxy Laminates Under Tensile Loading at Quasi-Static and High Rates." In: *Proceedings of the American Society for Composites Seventh Technical Conference*, pp. 1041-1050.
- Sun, C.T. and Chen, J.L., 1989, "A Simple Flow Rule for Characterizing the Nonlinear Behavior of Fiber Composites," *Journal of Composite Materials*, Vol. 23, pp. 1009-1020.
- Taylor, L.M. and Flanagan, D.P., 1989, " Pronto 3-D: A Two Dimensional Transient Solid Dynamics Program," SAND86-0594.

- Williams, J.G. and Rhodes, M.D., 1982,"Effect of resin on Impact Damage Tolerance of Graphite/Epoxy Laminateds" in Composite Materials: testing and Design (sixth Conference), ASTM STP 787 edited by Daniel, I.M., *American Society for Testing and Materials*, pp. 450-480.